Hydrogen transport on graphene: Competition of mobility and desorption

V. A. Borodin,[1,*] T. T. Vehviläinen,[2] M. G. Ganchenkova,[2] and R. M. Nieminen[2]
[1]*NRC Kurchatov Institute, Kurchatov Sq. 1, 123182 Moscow, Russia*
[2]*Aalto University School of Science, P.O. Box 11100, FI-00076 AALTO, Espoo, Finland*
(Received 15 May 2011; revised manuscript received 18 June 2011; published 18 August 2011)

The results of molecular dynamics (MD) simulations of atomic hydrogen kinetics on graphene are presented. The simulations involve a combination of approaches based on Brenner carbon-hydrogen potential and first-principles force calculations. Both kinds of MD calculations predict very similar qualitative trends and reproduce equally well the features of hydrogen behavior, even such sophisticated modes as long correlated jump chains. Both approaches agree that chemisorbed hydrogen diffusion on graphene is strongly limited by thermal desorption. This limitation rules out long-range diffusion of hydrogen on graphene but does not exclude the short-range hydrogen diffusion contribution to hydrogen cluster nucleation and growth.

DOI: 10.1103/PhysRevB.84.075486 PACS number(s): 68.65.Pq, 68.43.Jk, 68.43.Nr, 61.48.Gh

I. INTRODUCTION

Hydrogen interaction with carbon surfaces is an active research topic motivated by broadly varying interests, from purely scientific (e.g., the problem of interstellar molecular hydrogen in astrophysics) to strongly technologic. In the last few years, interest in the topic has been accentuated by demonstration of the possibility of creating individual layers of sp^2-bonded carbon (graphene), a material with unique properties that are expected to have many high-tech applications.[1,2] For example, the extremely fast charge carrier transport in graphene makes this material very promising for the development of novel carbon-based nanoelectronic components, whereas the possibility of covering practically the whole graphene surface with hydrogen[3–5] opens a way to use graphene as an efficient hydrogen storage material.

The real-life application of graphene, even leaving aside technological challenges of producing sufficiently large sheets of high-quality samples,[6] will depend very much on its functional possibilities. For example, applications in microelectronics can be largely expanded if one were able to convert graphene, which is basically a semimetal,[1] into a semiconductor, preferably with an adjustable band gap. The complete hydrogen coverage of graphene is expected to open the band gap well above the values demanded by conventional electronics (∼3.5[4,7] to ∼5.5 eV,[8,9] as predicted by first-principles density functional theory (DFT) calculations in different approximations). One way currently considered of adjusting the band gap width is partial graphene coverage with hydrogen.[10,11] Some microelectronics applications might profit from the well-defined electron levels close to the Fermi energy introduced by hydrogen chemisorbed on graphene.[12–14] These defect levels become isolated when hydrogen adsorption opens the band gap.[12,14–16] The effect is similar to that observed for carbon nanotubes, in which hydrogen atoms also introduce isolated levels in the middle of the band gap.[17,18] It has been demonstrated that clustered hydrogen atoms on nanotubes introduce multiple levels in the band gap,[18] which also can be expected for hydrogen clusters on graphene. Thus a proper tuning of nanoisland size and surface coverage patterns opens a way to band gap engineering via hydrogen clustering, either alone[19] or assisted with mechanical deformation, such as deliberate rippling[20] or elastic straining.[9]

Similarly, hydrogen storage on graphene, in spite of excellent gravimetric characteristics, will be seriously considered only provided one solves the well-known dilemma encountered in other carbon nanostructures (nanotubes and fullerenes)—that is, reconciling the high storage efficiency (sufficiently strong carbon-hydrogen binding) at room temperature with the reasonable ease of reversible hydrogen charging/discharging. Indeed, the most recent evaluations[21,22] give the potential barrier of ∼1.1 eV for chemisorbed hydrogen dissociation from graphene. With this desorption energy, it is easy to verify that the average lifetime of individual hydrogen atom on graphene at room temperature is less than a week. Experimentally, at surface coverage excluding clustering of hydrogen atoms (∼0.03%), 80% of hydrogen predeposited on graphite surface at 210 K is removed by 10 minutes of annealing at room temperature.[23] At such temperatures, there is little difference between graphene and graphite, so this result is equally representative for hydrogen desorption from graphene. On the other hand, the estimated hydrogen dissociation energy from fully hydrogenated graphene (graphane) is close to 2 eV[24] allowing reliable hydrogen storage at room temperature for many days,[5] but making hydrogen release problematic. The reported regime of full hydrogen discharge from graphane (24 hours at 450 °C[5]) is well inferior to the application-relevant hydrogen refueling rate (see, e.g., Ref. 25). An interesting possibility of solving the dilemma could be the partial graphene coverage with hydrogen islands, because the efficiency of hydrogen binding can be tuned by the adjustment of hydrogen island size and shape.[14,19,23,26,27]

The creation of hydrogen nanoislands on carbon can be beneficial even in those applications in which the hydrogen interaction with carbon surfaces is undesirable (e.g., in fusion facilities). Graphite coating is among the possible concepts of tokamak vacuum chamber inner wall protection. During the tokamak operation, high fluxes of various hydrogen isotopes are unavoidable, leading to various kinds of coating damage. In particular, hydrogen atoms deposited on carbon surfaces can return to the plasma, contributing to plasma cooling. The first wall operation temperatures are expected to reach several hundreds degrees Celsius, so the above-cited desorption barrier of 1.1 eV is not a serious obstacle for hydrogen adatom detrapping. The clustering of hydrogen atoms, increasing their

binding with the carbon surface, might be helpful in improving hydrogen retention on the first wall inner surface and reducing detrapping. However, the efficiency of this reduction is not easy to estimate, keeping in mind that already at ∼450–500 K[28,29] closely lying hydrogen atoms on graphite surface tend to pair into molecules that have no real binding to carbon substrates.

To achieve nanoisland nucleation, it is necessary, first of all, to deposit hydrogen onto graphene surface and, second, to promote the clustering of deposited hydrogen atoms. In the last decade, it has become clear that hydrogen deposition onto carbon is not technologically difficult.[28,29] The trapping of atomic hydrogen on a carbon surface was shown to be energetically favorable for practically all sp^2 carbon phases (from fullerenes and nanotubes to bulk graphite).[30,31] The only problem is overcoming a surface adsorption barrier (∼0.2 eV for graphene/graphite), which has been predicted theoretically[32] and recently confirmed experimentally.[33] The current technique of hydrogen deposition onto carbon (both graphite[23,28,29,34] and graphene[5]) uses "hot" hydrogen sources that supply hydrogen atoms with the average kinetic energy comparable to the adsorption barrier height, but other technological tricks might be suggested in the future. For example, according to recent first-principles estimates,[35] hydrogenation might be achieved even in a molecular gas via the dissociative adsorption catalyzed by sufficiently strong electric fields.

On the contrary, controlled nanoisland nucleation and growth on graphene is a challenge. With standard hydrogen deposition techniques (from gas phase or plasma) at relatively low temperatures (well below room temperature), hydrogen is deposited randomly, and the most probable clusters at intermediate H coverage (1–2 at.%) are hydrogen dimers[23,34,36] that form presumably when a hydrogen atom is deposited next to an already chemisorbed atom. Naturally, at hydrogen coverage of tens of atomic percent, the regions of closely lying hydrogen atoms occupy large parts of the graphene surface, but these are percolated irregular-shaped areas, rather than individual islands.[23,37] It remains unclear whether it is possible to promote and control nanoisland nucleation and growth at lower than several percent surface coverage.

A common trick to nucleate adatom islands on bulk material surfaces is the activation of adatom surface diffusion. As we demonstrated earlier,[18] on carbon nanotubes diffusion can efficiently promote hydrogen clustering. However, in the case of nanotubes, the energy barrier for hydrogen diffusion was found to be ∼0.3 eV lower than the energy of hydrogen thermal desorption from the studied nanotube surface (∼1.4 eV[18]), allowing us to neglect the desorption at temperatures below 500 °C. With graphene, the situation seems to be more complicated. The above-mentioned hydrogen detrapping energy from graphene, ∼1.1 eV, is notably lower than for nanotubes. Thus, the efficiency of cluster formation by surface hydrogen diffusion (the process is often referred to as the Langmuir–Hinshelwood mechanism, especially where hydrogen dimer formation on surfaces is concerned) can be strongly suppressed by competing thermal desorption, if the hydrogen migration barrier on graphene is comparable to or larger than the desorption barrier.

Although literature data on the hydrogen desorption barrier agree quite well, this is not the case for the hydrogen migration barrier. The majority of hydrogen migration barrier calculations employed very small simulation cells (16–32 atoms), which did not fully take into account the relaxation of two carbon atoms between which the hydrogen jump occurs. Meanwhile, as verified for the case of desorption, relaxation of carbon atoms close to the hydrogen atom is essential: the hydrogen atom does not bind to graphene without it and shows no attachment/detachment barrier.[14,38] Moreover, as pointed out in Ref. 32, there is no binding between a H atom and a perfectly flat graphene sheet at the midpoint of a diffusion jump along a C-C bond, which means the neglect of carbon lattice relaxation makes hydrogen diffusion simply impossible.

The largest DFT-based values for the hydrogen migration barrier (1.3 eV[39] or 1.14 eV[23]) exceed the desorption barrier and thus practically rule out the possibility of hydrogen migration on graphene. However, most calculations predict the hydrogen migration barrier to be lower than that for desorption. In some cases, the predicted barriers (1.035,[40] 1.01,[16] 0.98,[22] or 0.94 eV[41]) are only slightly lower than the detrapping energy; in others, the difference is more pronounced. For example, the diffusion barrier of 0.78 eV has been predicted by DFT calculations[42] and tight-binding molecular dynamics simulations.[43] Very recently, it has been claimed that the hydrogen diffusion barrier can be as low as 0.29 eV.[44] DFT calculations in the local density approximation[45] predict higher hydrogen migration and desorption barriers (1.19 eV and 1.32 eV, respectively) than in other methods, but still migration is favored compared with detrapping. As can be seen, even where the hydrogen migration barrier is lower than that for detrapping, a hydrogen atom is not expected to travel very far on graphene/graphite, but where hydrogen clustering is concerned, even limited diffusion is beneficial and allows a newly deposited hydrogen atom to reach the nearest available cluster and become stabilized against thermal detrapping.

Summing up, the current state of the art indicates that hydrogen transport on graphene involves strong competition between diffusion and detrapping. The kinetics of this competition has not been studied in any detail. The current work has been undertaken to better understand the physical features of hydrogen diffusion on a graphene surface, to investigate the competition between hydrogen diffusional transport and thermal desorption, and to clarify the possibility of hydrogen nanoisland formation on graphene/graphite via diffusion-assisted clustering of chemisorbed hydrogen adatoms.

II. SIMULATION TECHNIQUES

The kinetics of hydrogen on graphene have been investigated using the molecular dynamics (MD) approach. Both the "classical" and first-principles treatments were used to cross-verify and supplement the results.

The "classical" counterpart of the study was implemented using the MD code PARCAS.[46] The interaction between carbon and hydrogen atoms was described with the semi-empirical Brenner potential[47] implemented in the code. The Brenner potential is an Abell–Tersoff kind of potential, which was developed especially for hydrocarbons and is a common choice for MD simulation of carbon-hydrogen systems. It combines good transferability between carbon systems with different hybridization of carbon atoms and provides the ability

to describe bond breaking and forming properly and high efficiency in terms of computational costs.

The simulation supercell had orthorhombic shape and periodic boundary conditions in all three dimensions. Considering the equilibrium distance between carbon atoms for this potential, $a = 1.45$ Å, the simulation cell sizes in x and y directions were selected equal to 87.04×50.26 Å, so as to accommodate a 1600-atomic graphene layer positioned in the $z = 0$ plane (in the Cartesian coordinate system with axes aligned along cell sides). The cell size in the z direction was arbitrarily set to 20 Å, which is much above the possible thermal vibration amplitude of a graphene layer at temperatures involved in the study. The simulation cell size was kept the same during simulation runs, implementing an NVT ensemble.

Temperature adjustment during simulations was achieved using the Berendsen thermostat[48] with a temperature relaxation time of 0.1 ps. Temperature-dependent adjustments of the simulation cell size were mostly not applied because the thermal contraction of graphene is low (the in-plane graphene thermal expansion factor for the interatomic potential used was estimated as roughly -3.4×10^{-6}/K in the temperature range of 1100–2000 K; cf. the first-principles DFT value of $-(1 \div 2) \times 10^{-6}$/K[49]). As verified in several dedicated runs, relatively small (within 0.5%) variations of the simulation cell size practically did not affect the hydrogen kinetics.

The MD time step used was equal to 0.2 fs, which was verified to provide smooth hydrogen trajectories, even at the highest studied temperature.

The graphene layer with a single hydrogen atom on it was subjected to long-term annealing at temperatures in the range of 1200–2000 K. The initial configurations for annealing at each studied temperature were either obtained by heating up a flat graphene layer from 0 K (within 100–150 ps) or borrowed from annealing runs at other temperatures (differing by no more than 100 K from the desired temperature). In the latter case, it took ∼1–2 ps to equilibrate the system to the desired temperature, which was negligible compared with the average hydrogen lifetime on the surface. The run duration at any particular temperature was determined by the necessity to accumulate reasonable statistics of both hydrogen detachment events and diffusion jumps. Typically, it took simulation times from 2 ns at the highest temperatures to tens of nanoseconds at lower temperatures. At temperatures below 1500 K, we had to use several runs starting from different configurations to accumulate sufficient detachment and jump statistics because, at long simulation times (above ∼10 ns in this temperature range), a sinusoidal instability arose in many (though not all) runs (see Sec. III B below for details), which completely suppressed both hydrogen diffusion and detachment. During each run, intermediate snapshots of the system configuration were saved at intervals of 0.4 ps, except for several runs dedicated to a detailed tracing of the hydrogen trajectory, for which a much shorter interval of 4 fs was applied. A typical instantaneous configuration of the investigated system at high temperatures is shown in Fig. 1. The graphene sheet is notably corrugated, in agreement with earlier simulations and analytical predictions.[50–52] Corrugations arise because atoms in a monolayer can be relatively easily displaced in the direction normal to the layer plane. Ripples and corrugations are

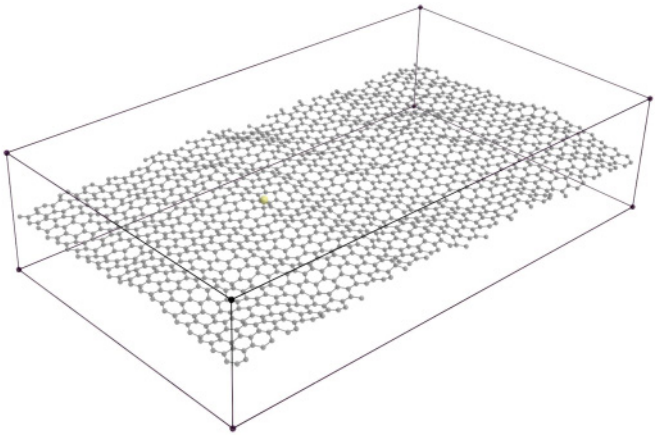

FIG. 1. (Color online) Snapshot of an instantaneous system configuration at 1700 K. Carbon atoms and hydrogen atom are shown as dark gray and light gray (yellow in color) spheres, respectively. The simulation box is also outlined.

expected to be universal features of graphene-like monolayer structures. For example, ripples have been experimentally observed in suspended graphene,[53] although in the reported experimental conditions (room temperature), they were hardly due to thermal vibrations.

The raw MD data were postprocessed to identify individual events of hydrogen detachment from and re-attachment to the graphene surface, as well as hydrogen movement events along the surface. Because of periodic boundary conditions, a detached hydrogen atom flies between the opposite graphene surfaces and is quickly recaptured, so that one MD run includes many detachment-reattachment events. Detachment events were fixed by the detection of either a freely flying hydrogen (i.e., hydrogen that had no carbon neighbors within the H-C interaction cutoff of 2 Å) or the sudden change of the graphene side occupied by hydrogen, which happened when the hydrogen atom flew from one side of the graphene sheet to the other between two consecutive configuration snapshots. An uncertainty arose for cases in which a detrapped and recaptured hydrogen atom crossed the distance between the graphene sheet and its periodic image an even number of times between consecutive snapshots. Although such events are definitely very rare, they cannot be completely excluded and might be one of the reasons for "long" hydrogen jumps (see Sec. III B below). Diffusion jumps of the hydrogen atom could be detected easily because any such event is accompanied with a change of the hydrogen nearest neighbor (NN) carbon atom.

The first-principles simulations were more restricted because of much stricter computer resource requirements compared with classical MD. The graphene layer consisted of 160 carbon atoms and one hydrogen atom in an orthorhombic supercell with dimensions 21.36×19.74 Å parallel to the graphene plane and 12.00 Å perpendicular to it. The calculations were performed using the DFT approach as implemented in the plane wave basis code VASP.[54,55] A spin-polarized version of DFT was used for the determination of hydrogen desorption and migration barriers; however, the dynamic behavior of hydrogen was found to be weakly affected by the account of spin polarization, and most of the MD calculations were done in non–spin-polarized mode to accelerate code

performance. The generalized gradient approximation with the exchange-correlation functional form of Perdew–Burke–Ernzerhof (PBE)[56] was applied. To represent the core ($1s^2$) electrons of carbon atoms, we used the projector augmented wave (PAW) method.[57,58] A kinetic energy cutoff of 400 eV and Fermi smearing of 0.1 eV were applied in all calculations. Sampling of the irreducible part of the Brillouin zone was performed with the use of a Monkhorst–Pack k-space grid[59] with $3\times3\times1$ points. The energy convergence with respect to k-points and cutoff energy was tested. On the basis of these tests, the estimated accuracy for energies is on the order of 0.01 eV, and structure relaxation accuracy is within 0.01 Å.

As with the classical MD, the NVT ensemble was used, but the simulation temperature was 3300 K (i.e., much higher than in "classical" simulations), so that both hydrogen desorption and diffusion events could be observed within the necessarily limited times covered (maximum 3 ps per MD run). In spite of being quite high, the simulation temperature is well below the graphene melting temperature, which, according to our preliminary estimates, exceeds 4000 K.

Migration barriers for hydrogen diffusion and hydrogen detachment barriers were estimated (only in DFT simulations) using the climbing image–nudged elastic band (CI-NEB) technique[60] or, where explicitly mentioned, the drag method.[61] To better understand the energetics of hydrogen diffusion, the potential energy surface (PES) for hydrogen over graphene was calculated. In these calculations, a hydrogen atom was placed in different positions of a regular hexagonal grid on top of the 160-atom graphene sheet and was allowed to relax only in the z direction. All carbon atoms were also allowed to relax, except for one carbon atom (located sufficiently far from the hydrogen), which remained fixed to prevent the shift of the graphene sheet as a whole.

III. RESULTS

A. Static properties of hydrogen atoms on graphene

Before studying dynamic hydrogen behavior, we verified equilibrium properties of a hydrogen atom on the surface for both the empirical potential and the first-principles approach. In agreement with the earlier DFT calculations, the ground state configuration of a hydrogen atom on graphene is the "on-top" location, with a single NN carbon atom [Fig. 2(a)]. This carbon atom sticks slightly above the graphene plane (by 0.13 Å in "classical" and 0.48 Å in DFT calculations), indicating a partial transition from sp^2 to sp^3 hybridization of carbon valence electrons. The binding energy of the hydrogen atom at the surface and the hydrogen-carbon distance for the Brenner potential are 1.36 eV and 1.32 Å, whereas the DFT calculation gives, correspondingly, 0.86 eV and 1.13 Å. The DFT binding energy value nearly exactly reproduces that of Ref. 62 and falls within 0.1 eV from the predictions of other authors (see Ref. 21 for a recent review).

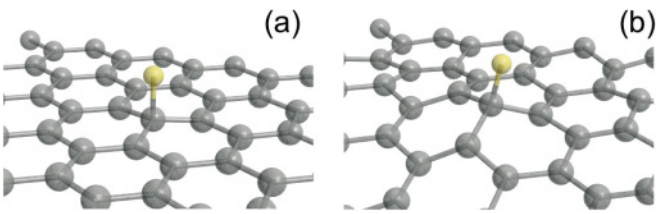

FIG. 2. (Color online) Hydrogen atom on graphene. (a) Equilibrium configuration at 0 K; (b) an example of instantaneous configuration during dynamic simulation with Brenner potential at high temperatures (here, 1400 K).

The CI-NEB DFT estimate of the hydrogen migration barrier for jumps to the first NN position is 0.99 eV (Fig. 3). The value falls between the available literature values discussed in the Introduction, being nearly the same as in Ref. 22. It is slightly less than the desorption barrier of 1.1 eV; the latter is, as expected, identical to that reported in the literature. It has been recently argued[44] that the hydrogen migration barrier on the order of 1 eV can be a gross overestimation because of the use of small simulation boxes. However, we do not observe the migration barrier reduction, despite our simulation box being bigger than that used in Ref. 44.

To gain better insight, the full potential energy surface of a hydrogen atom on graphene was calculated (Fig. 4). It clearly shows that, in agreement with earlier papers,[22,42,45] the hydrogen jump between NN carbon atoms requires the lowest energy. The energy profiles for hydrogen jumps according to PES are shown in Fig. 3. As can be seen, both CI-NEB and PES predict essentially the same energy barrier height for the 1NN hydrogen jump, although the CI-NEB energy profile is noticeably broader. It is also seen that a direct hydrogen jump to the 2NN carbon requires overcoming a higher barrier than a sequence of two 1NN jumps (as suggested earlier in Ref. 42).

An interesting feature of the potential energy surface is the double-hump hydrogen energy profile observed for the trajectory connecting 3NN carbon atoms, as shown in Fig. 3. A similar double-hump profile was obtained earlier[42] by the NEB method, although the predicted energy maximum was lower (0.95 eV[42]) than in the current study. This energy maximum was interpreted in Ref. 42 as the barrier for the 3NN hydrogen jump. This, however, is misleading, because

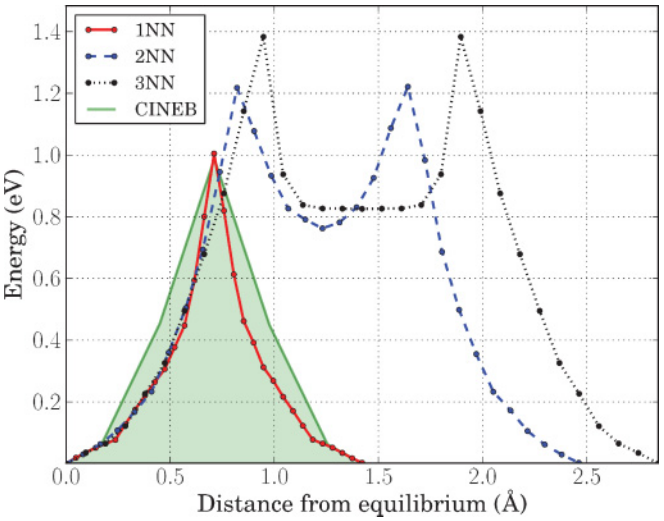

FIG. 3. (Color online) The minimum energy paths for H atom on graphene. Included are the 1NN jump barrier profile predicted by CI-NEB (solid line with shaded background) and PES profiles along the lines connecting 1NN, 2NN, and 3NN carbon atoms (solid, dashed, and dotted lines with circle markers, respectively).

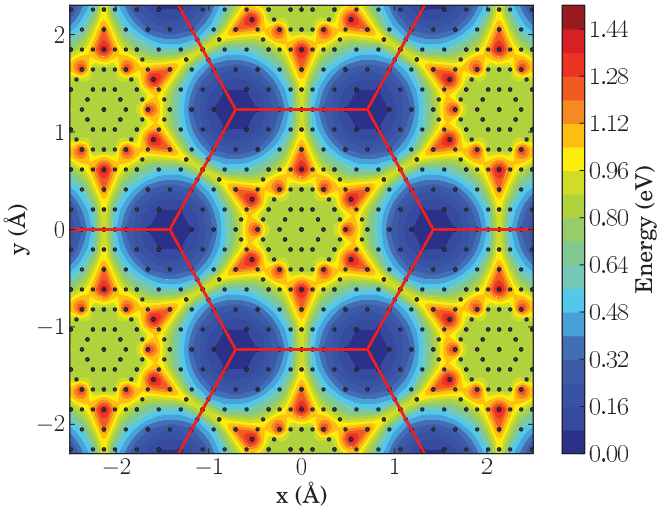

FIG. 4. (Color online) The potential energy surface for a H atom on top of a graphene sheet. Carbon network is marked with straight lines. Open circles (or black dots in color version) indicate calculation points. The correspondence between the shades of gray (colors in color version) and hydrogen energies is shown in the scale bar at the right of the figure.

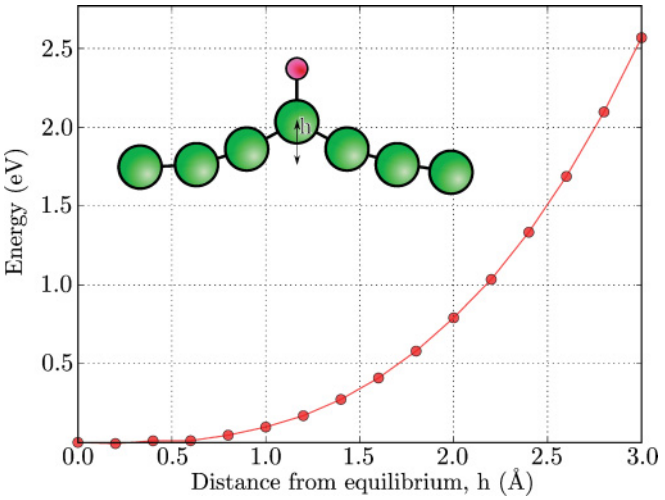

FIG. 5. (Color online) The potential energy increase of the hydrogen atom in the "drag" simulation experiment.

in the middle part of a hexagonal carbon ring, the hydrogen atom is not trapped and the bottom of the PES energy well is essentially the hydrogen binding energy. The energy maximum of 1.4 eV should be considered rather as the detrapping energy for the hydrogen atom moving toward a 3NN carbon neighbor. Note, however, that this is only true for adiabatic movement of the hydrogen atom. In dynamic simulations, the situation is more ambiguous, and jumps over the hexagon center are possible, as discussed in more detail in Sec. III B below.

With high flexibility of the graphene sheet in the direction normal to its plane (cf. Fig. 1), it is unclear whether the "ideal" (i.e., predicted by static relaxation) binding and migration energies are fully relevant for the estimation of hydrogen lifetime and mobility in the chemisorbed state. This doubt is supported by the outcome of a DFT-based simulation, wherein hydrogen atom detachment was imitated with the help of the drag method. That is, the H atom was pulled away from graphene starting from its equilibrium position on the surface in steps of 0.2 Å, with intermediate relaxations of carbon atom positions at each step. During the intermediate relaxation, the position of the H atom, as well as that of one carbon atom sufficiently far away from the H, were fixed. Because graphene is very elastic, the bond between H and the nearest carbon atom would not break easily, as shown in Fig. 5. In fact, the breaking point depended on the size of the supercell: the bigger the supercell, the more strongly the hydrogen bent the graphene sheet. In the 160-atom supercell, the hydrogen atom could be pulled off by more than 3 Å before the C-H bond broke. The energy required to break the C-H bond in this case exceeded 2.5 eV, being much higher than that predicted by CI-NEB. A similar trend of carbon atom shift behind the dragged hydrogen atom was reported earlier in Ref. 38, but there the effect was much less pronounced because of the very small model size (8 atoms per graphene sheet).

The drag simulation results suggest that the transverse flexibility of graphene can be an important factor affecting the apparent detachment and migration barriers of hydrogen on the graphene surface. At temperatures in which one expects hydrogen diffusion to be observable, the instantaneous local environment of carbon atoms is far from purely planar, whether these atoms have hydrogen attached or not [see Fig. 2(b)]. Correspondingly, the instantaneous local potential energy surface for a hydrogen atom can be notably different from that shown in Fig. 4. The latter consideration is indirectly supported by the first-principles simulations of Ref. 20, indicating that the local curvature of graphene caused by rippling noticeably affects the efficiency of carbon-hydrogen binding. Being much lighter than carbon, hydrogen makes multiple on-spot oscillations during one transverse oscillation of a carbon atom, probing various escape possibilities from its carbon neighbor. One can expect that in a permanently changing local environment, hydrogen detachment from the neighboring carbon would involve energy barriers different from those predicted by CI-NEB calculations. With this in mind, we discuss the outcome of the full MD calculations.

B. "Classical" MD

Calculations with the semi-empirical potential for all studied temperatures (1200–2000 K) demonstrated qualitatively very similar hydrogen behavior, as exemplified in Fig. 6. That is, hydrogen is efficiently trapped by graphene and, even at the highest temperature considered, remains attached to it for a sufficiently long time (at least 1 ps) to be securely identified as trapped on-site. At any snapshot of the system configuration, the hydrogen-carbon bond is easily identified because no more than one carbon atom is present within the potential cutoff distance (0.2 nm) of the hydrogen atom. In what follows, such a carbon atom will be denoted as C_1.

In quantitative terms, the hydrogen behavior is illustrated in Fig. 7 for a simulation temperature of 1400 K. As can be noticed in Fig. 7(a), the oscillation of the C_1-H bond length is faster than the oscillation of bond lengths between C_1 and any of its carbon neighbors (C_2), which is readily explained by the notable mass difference between hydrogen and carbon. To compare, the C_1 oscillation in the z direction (transverse

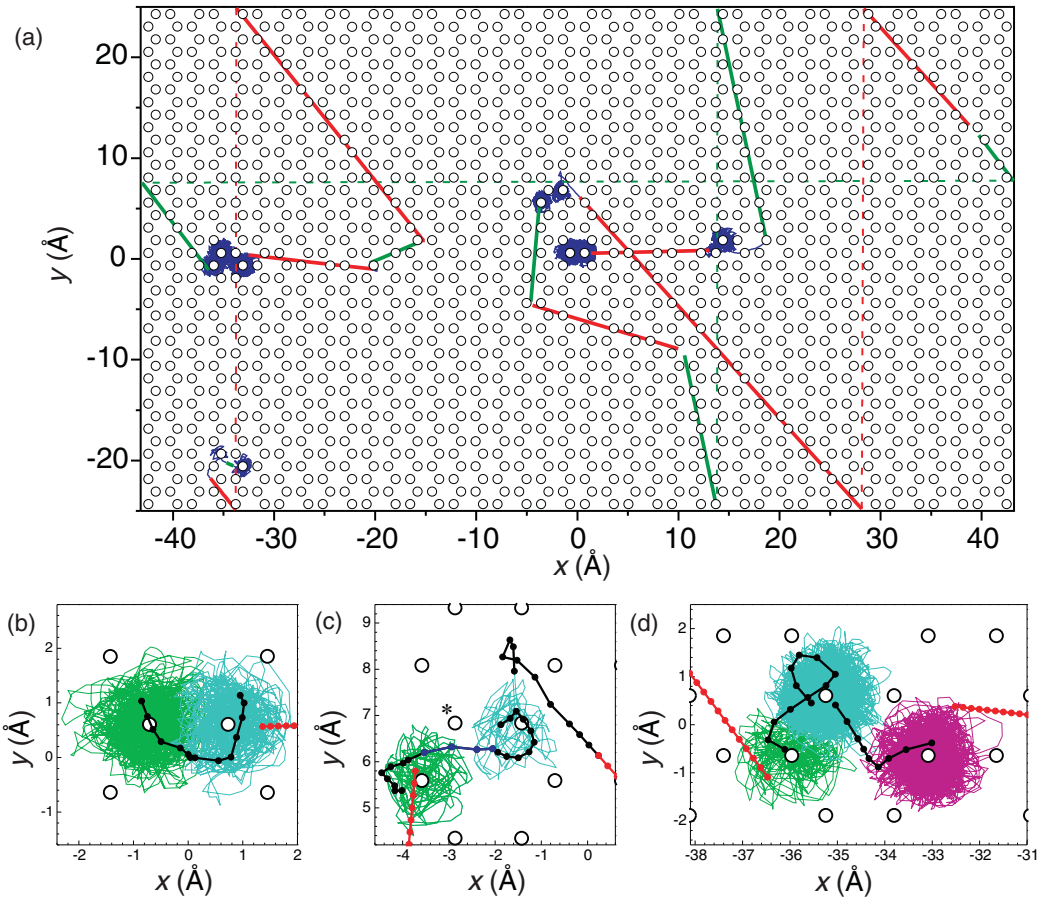

FIG. 6. (Color online) (a) An example of hydrogen atom trajectory corresponding to an 80-ps-long simulation at 2000 K viewed normal to the *x*-*y* plane. The initial hydrogen position is at the center of the simulation cell. When the hydrogen is attached to the graphene, its trajectory (dark blue in color) remains close to carbon lattice sites (small hollow circles), whereas the freely flying hydrogen moves along thicker straight lines of different shades (in color—red and green), allowing differentiation between the "up" and "down" flight directions. Thin dashed lines connect the trajectory points at the opposite sides of the simulation cell to guide the eye. (b–d) The enlarged trajectory parts demonstrating 1NN jump (b), 2NN jump (c), and a sequence of 1NN and 2NN jumps (d). The trajectory parts associated with different carbon atoms are shown in light gray (in color version—green, light blue, and violet), whereas those corresponding to hydrogen transitions from one atom to another are shown as thick black lines marked with dots identifying hydrogen positions in consecutively saved snapshots (separated by 4 fs). The freely flying H atom trajectories are straight dark gray (in color—red) lines. In (c), the central part of the jump trajectory, shown in lighter shade of gray (blue in color), indicates hydrogen association with the carbon atom on the site marked with an asterisk.

to the graphene plane) occurs on a notably longer time scale [Fig. 7(b)].

Instructive information for predicting hydrogen mobility can be obtained from the kinetics of H-C_1-C_2 dihedral angles (i.e., the angles between the H-C_1 and C_1-C_2 bonds). When a hydrogen atom jumps to a C_2 atom, the H-C_1 bond strongly inclines toward the C_1-C_2 bond, so that in the jump saddle point the angle between the bonds falls to less than 60°. An example of H-C_1-C_2 dihedral angle variation with simulation time at 1400 K, shown in Fig. 7(c), demonstrates that H-C_1-C_2 dihedral angles remain well above that required for a successful jump. In other words, diffusion jumps at this temperature involve strong fluctuations in the H-C_1-C_2 dihedral angles and can be expected to occur relatively rarely.

As can be seen in Fig. 7, even the largest stretching of the H-C_1 bond length is typically well below the interaction cutoff of 2.0 Å, so that hydrogen detachments are also infrequent. When a detachment does happen, the hydrogen escape directions seem to be completely random. Because of the periodicity of the simulation cell, the freely flying hydrogen atom reaches the graphene sheet from the opposite side and, as a rule, is quickly retrapped—either immediately or at higher temperatures after one or two reflections (see Fig. 6). Interestingly, such reflections are never mirror-like; rather, there seems to be no correlation between either polar or azimuthal angles of the falling and reflected particle trajectories.

The distributions of hydrogen lifetimes (intervals between consecutive trapping and detrapping events) are quite broad in the whole temperature range studied [Fig. 8(a) and Table I]. Nonetheless, the plot of the average lifetime versus the inverse temperature (Fig. 9) can be reasonably well approximated by a linear relation with the activation energy for hydrogen detrapping of 1.26 eV—that is, slightly less than the ideal hydrogen detrapping barrier for classical potential reported in Sec. III A.

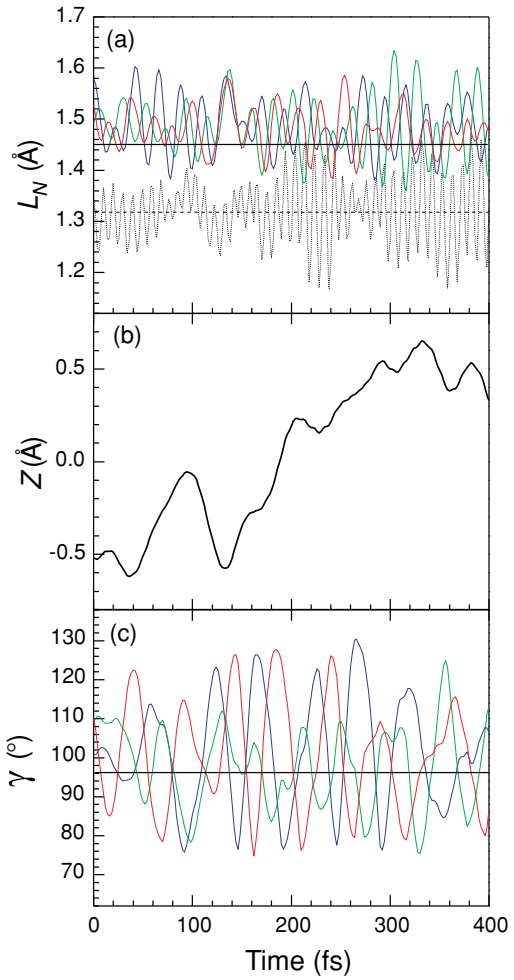

FIG. 7. (Color online) Various carbon and hydrogen parameters vs. time at 1400 K. (a) C_1-H (dash) and C_1-C_2 (solid) bond lengths, L_b; (b) z coordinate of C_1; (c) H-C_1-C_2 dihedral angles γ. Three solid curves in panels (a) and (c) correspond to different C_2 neighbors of C_1; curves for the same neighbors have the same color in both figures (in color version). Horizontal lines in these figures indicate the equilibrium values of corresponding parameters. All results are from MD simulations with Brenner potential.

While staying attached to graphene, a hydrogen atom is able to move via diffusion jumps. The average number of diffusion jumps made by a hydrogen atom during its lifetime on the surface is close to one, slightly increasing as temperature decreases (compare Tables I and II). However, depending on hydrogen lifetime on the surface, the number of jumps varies and can reach 7–10 for relatively long lifetime events [Fig. 8(b)].

The observed dominant mode of hydrogen diffusion is the jump to the 1NN position, but the correlated jump chains over two to five C-C bonds in the underlying graphene lattice are also regularly observed. The relative share of these jumps is ∼10–20% (see Fig. 10), with no evident temperature dependence. Typically, the longer the jump chain, the lower its frequency. Although we did not calculate the "ideal" hydrogen migration barriers for the Brenner potential, hydrogen behavior is qualitatively compatible with the DFT data described in Sect III A. Keeping in mind Fig. 4, one would expect that jumps over several carbon bonds occur as sequences of 1NN jumps. The only exception seems to be the jump to the 3NN position, which can occur also as a direct transition between the initial and the final configurations. Such a transition requires higher energy, but avoids following a curved trajectory, as is characteristic for a chain of 1NN jumps. With our standard MD procedure, it was difficult to unequivocally specify, whether the jumps occur directly or via a chain of consecutive 1NN jumps because most of the jumps happened completely between saved configuration snapshots, and only occasionally intermediate jump configurations were fixed. These rare events indicated, however, that both jump modes are possible.

To make things clearer, a 80-ps-long MD run with very frequent intermediate saves (each 4 fs) was undertaken, with the output shown in Fig. 6. As can be easily noticed, the trajectories for hydrogen diffusion jumps do not follow the lowest energy pathway predicted by the NEB method on the "ideal" carbon lattice. Nonetheless, Fig. 6(c) shows the 2NN jump trajectory that approximately follows the underlying graphene lattice. On the other hand, Fig. 6(d) shows a 2NN jump that avoids the intermediate carbon atom, starting toward the 3NN carbon atom and then changing the target for a 2NN carbon atom. Although it looks exotic, the jump mechanism is consistent with the double-hump shape of the jump barrier in the 3NN direction. Moving toward a position above the center of a carbon hexagon, a hydrogen becomes weakly (if at all) bound to its former carbon neighbor, so its fate depends on the presence or absence of another carbon atom nearby, which can be any of the five remaining carbon atoms in the hexagon. That is, traveling above the hexagon center, the hydrogen atom can make a jump not only to the 3NN position, but also to a 2NN [as in Fig. 6(d)] and even a 1NN position. The regular MD simulations give examples of all such jumps, even though only a small fraction of all jumps allows tracing the intermediate jump configurations. On the other hand, if no carbon atom is sufficiently close, the hydrogen atom flies away [a detachment event of this kind can be seen in Fig. 6(c)].

Sometimes diffusion jumps in which the hydrogen atom travels over more than five C-C bonds at once are observed. In some cases, these moves are clearly identified as sequences of 1NN, 3NN, or both kinds of jumps. However, particularly long jumps occurring without any trace in intermediate configuration snapshots are most probably artifacts resulting from hydrogen detrapping and retrapping on the same graphene sheet side after a reflection from an "image" layer. In very unfavorable cases in which the hydrogen atom detaches from graphene in a nearly normal direction, it takes only several tens of femtoseconds to reach the "image" sheet and return, with the whole detachment event falling completely between consecutive configuration snapshots. No attempt to determine the true share of such artificial "jumps" from the MD calculation was undertaken because it would require prohibitively large computational resources and time. In any case, they are too rare to affect noticeably either the calculated hydrogen lifetime or the jump statistics.

To quantify the frequency of hydrogen diffusion jumps, we employ the on-site residence time, defined as the time between consecutive jumps within hydrogen lifetime on graphene, including the time between hydrogen capture and the first jump. The statistics of on-site residence times at different

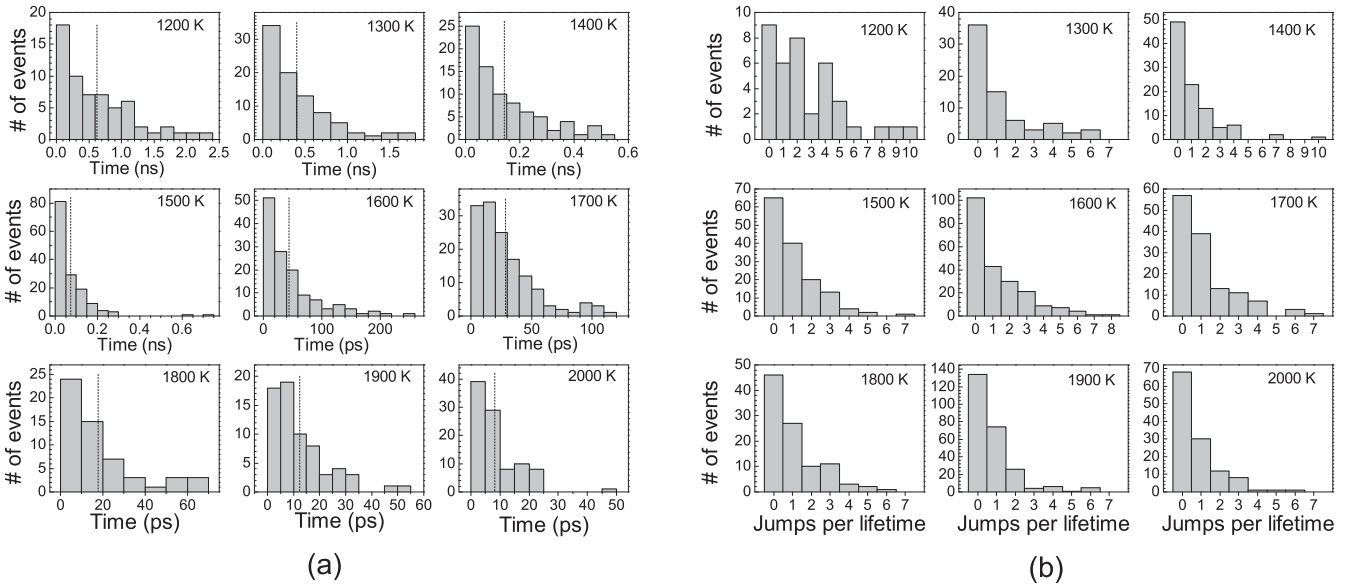

FIG. 8. Distributions of hydrogen lifetimes (a) and hydrogen diffusion jumps per lifetime (b) at different temperatures, as observed in MD simulations with Brenner potential. The mean values in (a) are shown with vertical dash lines.

temperatures is summarized in Table II. Temperature dependence of the average on-site residence time is plotted versus the inverse temperature in Fig. 9 and, when approximated by a straight line with the least squares fit, gives an apparent activation barrier of 1.14 eV.

The obtained activation energy for the on-site residence time can be considered a close approximation for the diffusion activation energy as well, because the inverse of the on-site residence time normally gives exactly the average jump frequency. But in the studied task, the on-site residence time cannot exceed the hydrogen lifetime on the surface. Thus the long on-site residence times give underweighted contributions to the average jump frequency compared with the standard situation. However, as one can judge from Fig. 11, the average jump frequency overestimation should not be too big. Even though some of the longer lifetime events do accommodate long on-site residence times, the majority of residence times, even for longer lifetimes, remains within a restricted range (below 50 ps at 1700 K or 25 ps at 2000 K).

The majority of calculations described above has been performed with the use of a simulation cell size corresponding to the equilibrium lattice parameter at 0 K. However, graphene is known to contract with an increase of temperature.[49] To estimate the effect of supercell size variation on hydrogen parameters, we performed two additional sets of simulations for temperatures 1200 and 1300 K. In the first set, the supercell sizes in the x and y directions were proportionally shrunk so as to reproduce the thermal contraction (∼0.5%, as determined in separate dedicated runs). In the second set, the simulation cell was, on the contrary, stretched by 0.15%, compared with zero-temperature equilibrium size. As can be seen in Fig. 9, the variation of cell size in such narrow limits practically does not affect either the hydrogen lifetime or on-site residence time. In fact, even tensile strains as high as 10% are not expected to change the hydrogen migration barrier by more then 10%.[22]

An unexpected effect observed in the current simulations is the development of a sinusoidal vibration instability. The effect is manifested in the gradual (within 2–5 ns) transformation of the irregularly corrugated graphene sheet, as shown in Fig. 1, into a sinusoidal running wave profile (Fig. 12). The amplitude of atomic vibrations in the z direction (i.e., normal to the "ideal" graphene plane) increases from 1–1.5 Å, as is

TABLE I. The hydrogen lifetime parameters obtained in MD simulations with Brenner potential. In the case of several runs at the same temperature, simulated time and event numbers are summed over all runs.

T (K)	Simulated time (ns)	No. of events	Average lifetime (ps)	Lifetime variance (ps)
1200	78	34	2.0×10^3	1.6×10^3
1300	62	69	8.0×10^2	8.0×10^2
1400	36	109	3.2×10^2	2.6×10^2
1500	24	146	1.6×10^2	1.6×10^2
1600	22	219	1.0×10^2	1.2×10^2
1700	8	130	59	56
1800	4	100	38	36
1900	6	272	21	16
2000	2	121	15	14

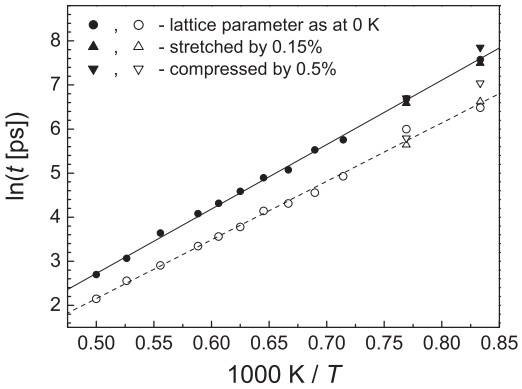

FIG. 9. The temperature dependence of the average hydrogen lifetimes on graphene (solid symbols) and the average hydrogen on-site residence times (open symbols). Circular symbols are from regular runs with the temperature-independent simulation box size. At the lowest two temperatures, the points for the runs in biaxially compressed (triangles down) and expanded (triangles up) simulation cells are added, as marked in the legend and explained in the text. Straight lines are least squares fits through regular data points (circles) only.

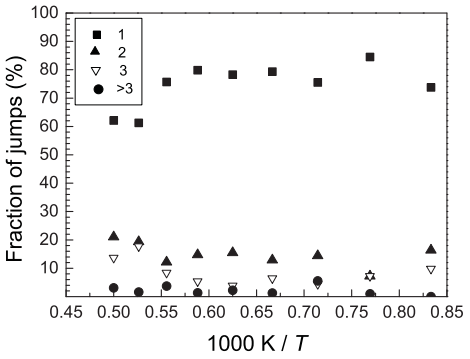

FIG. 10. The relative frequencies of different jump lengths (the number of C-C bonds traveled during the jump, as indicated in the legend) at different temperatures.

typical for thermally induced ripples, to nearly 6 Å in the fully developed sinusoidal mode. The frequency spectrum of an (arbitrary) carbon atom vibration in the z direction shows a pronounced difference between the random thermal vibration mode and the sinusoidal mode (see Fig. 13). Whereas, in the first case, the spectrum is characterized by multiple peaks at different frequencies, the well-developed sinusoidal vibration is characterized by the unique frequency.

The fact that graphene can undergo a vibrational resonance is interesting, but not really extraordinary in itself; any sufficiently big elastic membrane can resonate under proper conditions. A remarkable thing is that the instability is not driven externally but is a self-organization effect. Overall, it looks like a typical Lyapunov instability, wherein a vibration mode with a certain wave vector gradually evolves to become the dominant mode. A lag time for the instability onset typical for this instability type is also clearly manifested. The variability of the lag time from run to run could be the reason why the instability was observed only in some of the simulation runs. The observed lag times were quite long (minimum 8–10 ns), so possibly runs in which no instability was observed were simply not long enough. However, the detailed mechanism of self-organization has not been addressed in depth in the framework of this study; hence, it is not yet clear whether the sinusoidal instability is an inevitable ultimate fate of strongly heated graphene or whether arises only under appropriate combinations of external conditions (e.g., graphene sheet size and/or shape, border clamping, temperature, etc.).

At the moment, only general remarks contributing to the clarification of the observed instability can be made. First, no evident correlation between the instability lag time and simulation temperature was noticed. The upper detected temperature limit for the instability was 1500 K, but it does not exclude instability at higher temperatures. The runs at 1600 K and above required only several nanoseconds to acquire the necessary hydrogen statistics, which might be insufficient for instability onset. The self-organized sine wave frequency in our simulation setup was in the terahertz range (cf. Fig. 13), and the wave vector was always along the $\langle 11\bar{2}0 \rangle$ direction, but the latter might be equally well because this direction is parallel to the longer side of the simulation cell. On the other hand, the instability seems to be sensitive to elastic deformation, even though in a counterintuitive way. Treating graphene as an ordinary two-dimensional membrane, it would be natural to expect that the stability loss is promoted by in-plane compression. But in our study, the simulation box was mostly slightly larger than it ought to be for the considered high temperatures. In those runs (at 1200 and 1300 K) where the box size was shrunk to compensate for

TABLE II. The hydrogen on-site residence parameters obtained in MD simulations with Brenner potential. In the case of several runs at the same temperature, jump numbers are summed over all runs.

T (K)	No. of jumps	Average residence time (ps)	Residence time variance (ps)
1200	61	654	562
1300	87	402	394
1400	126	138	133
1500	160	74.4	92.3
1600	279	43.6	46.9
1700	141	28.3	24.8
1800	107	18.2	17.2
1900	200	13	10.7
2000	88	8.5	7.4

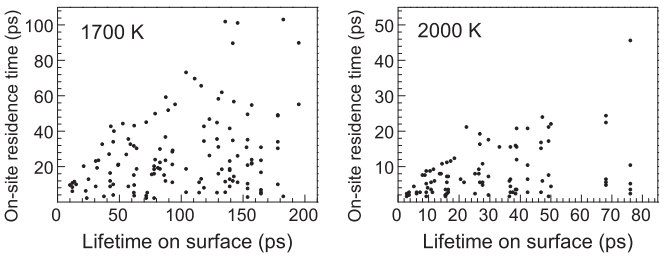

FIG. 11. The distributions of on-site residence times as a function of the hydrogen lifetime on the graphene surface for two simulation temperatures (as indicated in figure legends). Because all hydrogen attachment events have different lifetimes, points with the same abscissa are from one and the same event. Shown are only those events in which at least one diffusion jump per lifetime has occurred.

thermal contraction, instability did not develop up to as much as 50 ns, when the collection of hydrogen jump statistics was terminated. On the contrary, a deliberate additional stretching of the graphene sheet systematically shortened the lag time. It could be that the instability is related to the reported trend of tensile strains to suppress the longitudinal acoustic phonon modes, while weakly affecting the out-of-plane mode,[9,63,64] but it is definitely not the so called "phonon instability" predicted in Ref. 63, because we remain well below the threshold biaxial strain (∼15–20%[64,65]) required for the latter. Long-wave out-of-plane vibrations superimposed over the irregular thermal motion of atoms are permanently present at all the studied temperatures, but their amplitude never exceeds ∼1.5 Å, unless sinusoidal instability starts.

In relation to hydrogen mobility, the sinusoidal instability development resulted in complete suppression of both hydrogen diffusion and detachment. This effect seems to be a consequence of the applied technique of temperature control. A thermostat keeps the average kinetic energy of atoms in the system at a certain level, implicitly assuming that the dominant mode of atomic motion is thermal vibration. When the graphene sheet undergoes sinusoidal vibrations as a whole, the average kinetic energy of an atom is a sum of that due to regular sine vibration and that due to thermal vibrations. Keeping this sum at a constant level means that, with an increase of the sine vibration amplitude, the kinetic energy contribution from thermal vibrations (which ultimately specifies the temperature) falls well below the nominal value. Visually, this is manifested as a nearly complete disappearance of irregular ripples; the surface of graphene vibrating in well-developed sinusoidal mode is perfectly smooth (cf. Figs. 1 and 12). Hence, for runs in which sinusoidal instability was observed, only the initial part with the transverse vibration frequency spectrum resembling that shown in Fig. 13(a) was used for the analysis of hydrogen detrapping and diffusion.

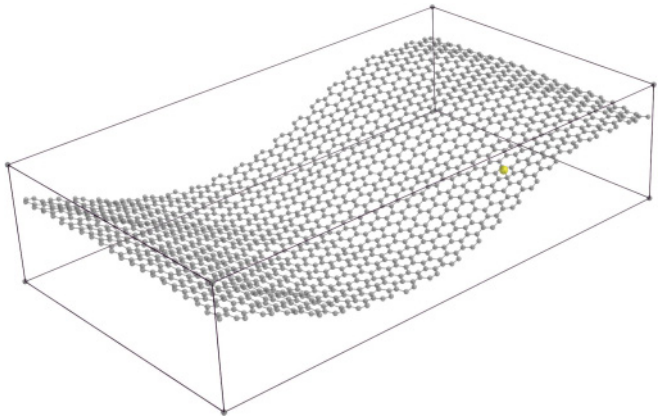

FIG. 12. (Color online) Snapshot of the instantaneous system configuration after development of a sinusoidal vibration instability. $T = 1300$ K.

C. MD-DFT

The MD-DFT simulations are too restricted to allow the accumulation of relevant statistics, but they provide a valuable reference for the verification of qualitative predictions of hydrogen behavior from "classical" MD simulations. The short interval between snapshots in MD-DFT simulations (typically 1 fs) provides a very detailed hydrogen trajectory. In spite of a quite noticeable difference in simulation temperatures, the qualitative predictions of both approaches closely correlate (cf. Figs. 6 and 14). In particular, in both approaches, hydrogen is observed to make only a few diffusion jumps before detrapping. As in "classical" MD, both 1NN and 2NN diffusion jumps, as well as longer correlated jump chains (up to several angstroms), are observed in MD-DFT. In most cases, the long jumps are chains of consecutive 1NN jumps, in which hydrogen quickly covers several interatomic distances, more or less following the bonds between NN carbon atoms.

A feature observed only in MD-DFT simulations is the presence of "ballistic" jumps. These are incomplete detachment events, wherein the hydrogen atom flies off of its carbon neighbor along a trajectory nearly parallel to the graphene sheet and is recaptured after traveling some distance in the collective field of many graphene atoms. As a result, the distance traveled by a hydrogen atom exceeds by far the carbon interatomic distance. In "classical" simulations such "ballistic" jumps are impossible because of the very short ranged H-C interaction.

MD-DFT simulation results provide deeper insight into the energetics of the hydrogen atom detachment from the graphene surface. Indeed, the commonly referred energy barrier of 1.1 eV for hydrogen detachment from graphene corresponds to the situation in which the graphene sheet remains flat during the detachment event and detachment occurs perpendicularly to the graphene surface. However, graphene at nonzero temperatures is corrugated, and most of the time, the local hydrogen atom environment is far from equilibrium, so the first condition is generally invalid in dynamic simulations. The second condition also does not hold because the hydrogen detachment trajectory is often pronouncedly inclined with respect to the z-axis. Evidently, both circumstances affect the value of the detachment barrier. To get a qualitative measure of the energy barriers for hydrogen desorption, we have performed a backward analysis of hydrogen kinetic energy variation during MD-DFT detachment events. That is, in each detachment event, a point of hydrogen trajectory sufficiently far from the graphene was selected, in which the hydrogen atom was moving free with a constant velocity, and the hydrogen kinetic energy was traced back along the trajectory

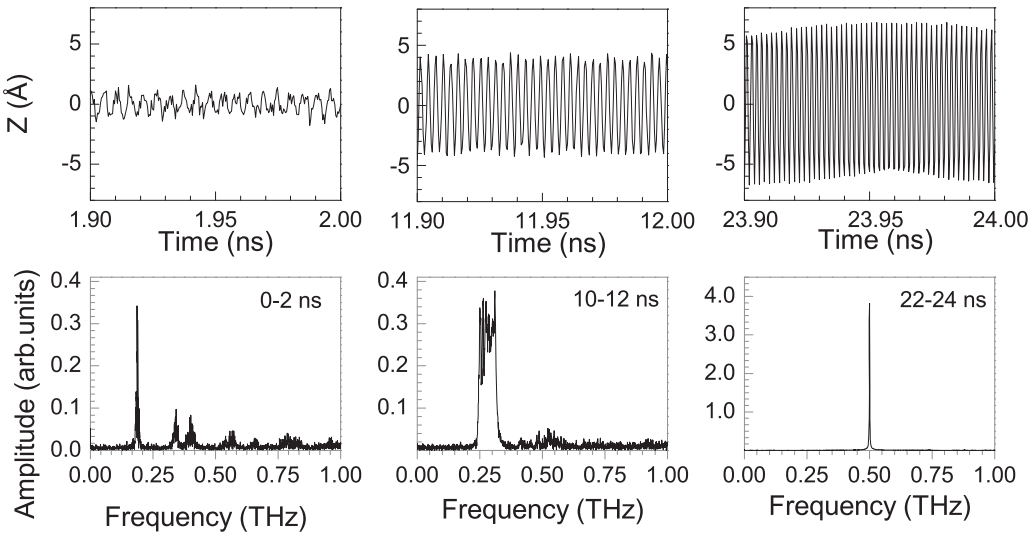

FIG. 13. Samples of carbon atom trajectory projections onto the z-axis at different times during the same simulation run at 1200 K (top row) and the corresponding temporal Fast Fourier Transform (FFT) amplitudes for these trajectories (bottom row). The sampling time ranges for FFT are indicated in the figure legends.

until it reached the maximum value. The difference of this value and the kinetic energy of free motion, ΔE, is a measure of the energy lost by the hydrogen atom to overcome the attraction barrier. As can be seen in Fig. 15(a), the scatter of data is noticeable and some jumps involve kinetic energy loss even below the "static" detachment barrier value. However, the average kinetic energy loss (1.2±0.4 eV) turned out to be quite close to the "static" value. In addition to the total kinetic energy loss, we plot in Fig. 15(a) the kinetic energy contribution ΔE_z from the velocity decrease in the z direction. When the hydrogen trajectory is nearly perpendicular to the graphene surface, $\Delta E_z = \Delta E$. However, in many events, the contribution to ΔE from H atom movement along the surface is comparable or higher than ΔE_z.

A similar procedure of kinetic energy tracing was applied to diffusion jumps and also demonstrated a spectrum of kinetic energy barriers, both higher and lower than the nominal migration barrier [see Fig. 15(b)]. However, in this case, the average kinetic energy variation (0.8±0.4 eV) can hardly be interpreted as a dynamic migration barrier because neither the initial nor the final kinetic energy maxima bracketing the saddle point (kinetic energy minimum) correspond to equilibrium positions. Nonetheless, the observed low kinetic energy variations (0.1–0.4 eV) in a number of jumps unequivocally indicate a strong effect of thermally induced graphene distortions on hydrogen jump kinetics, as shown in Fig. 16.

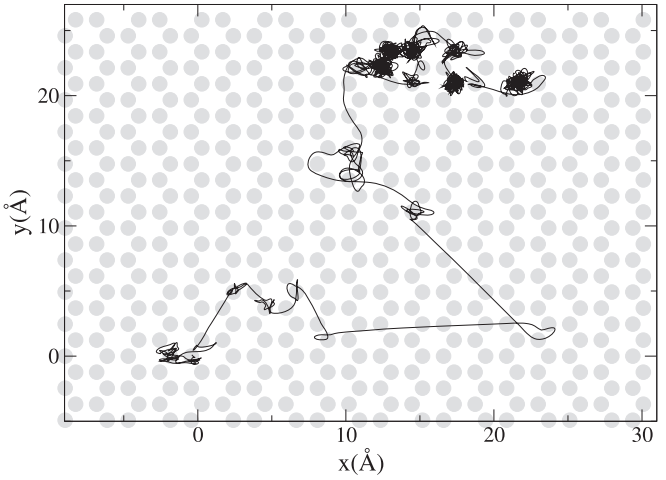

FIG. 14. Example of a hydrogen trajectory in one MD-DFT run projected onto the x-y plane. Graphene lattice sites are marked by background gray circles. The straight trajectory sections correspond to free hydrogen flights between opposite graphene surfaces.

IV. DISCUSSION

Following the standard practice of MD simulations, all calculations in this paper are performed at rather high temperatures to accelerate system kinetics. Even tens of nanoseconds of simulated times require a lot of computational effort. However, temperatures in practical applications clearly are never so high, so we discuss how the observed trends can be extrapolated to lower temperatures.

First, we consider how far a hydrogen atom can move during its lifetime on graphene. As seen in Fig. 8(b), the probability that a hydrogen atom deposited onto a graphene sheet makes no jumps at all during its lifetime is relatively high (roughly 50%, whatever the temperature). When these events are excluded, the average number of jumps per lifetime (n_D) tends to grow with a temperature decrease. The reason is clear from Fig. 9: when temperature decreases, hydrogen lifetime grows faster than the interval between diffusion jumps. To better quantify the effect, we present in Fig. 17 the calculated average number of hydrogen jumps per lifetime, considering only those lifetimes in which at least one diffusion jump has occurred. The data points in Fig. 17 suffer a large scatter, which is not unexpected. The reliable values of n_D require very accurate distributions of jump numbers per lifetime, which imply better statistics than that shown in Fig. 8(b), especially at lower temperatures. Nonetheless, there is a clear

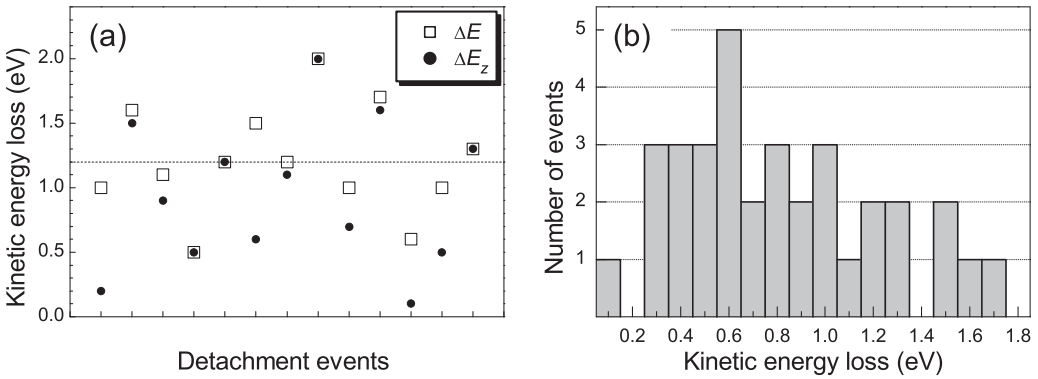

FIG. 15. (a) Kinetic energy loss in several H detachment events (dashed line is the average of ΔE over all events). (b) Histogram of kinetic energy loss in several jump events.

trend of an increase of n_D with a decrease of temperature. A straightforward extrapolation to room temperature according to the trend line shown in Fig. 17 gives $n_D \sim 250$. Keeping in mind that the average distance covered by a diffusing particle scales as the square root of the jump number, the estimate above indicates the ability of a hydrogen atom to travel at low temperatures at least a couple of nanometers before detachment. The long-range diffusion of hydrogen atoms (for tens of nanometers or more) can, naturally, be ruled out even at these temperatures.

Strictly speaking, hydrogen mobility at low temperatures can be modified by quantum effects. According to Ref. 43, below 600 K, quantum corrections to the vibrational behavior of chemisorbed hydrogen decrease the hydrogen migration barrier, implying an additional increase of distance traveled by a hydrogen atom. However, the barrier change is relatively small (∼10%), and this increase does not change the conclusion above.

In terms of nucleation and growth of hydrogen nanoislands on graphene, even limited surface mobility of hydrogen is helpful. Quite generally, cluster nucleation in a supersaturated solution of monomers starts from the formation of dimers. It is often assumed that to create a hydrogen dimer on a carbon surface, a hydrogen atom should be deposited in the immediate vicinity (within one to three NNs) of another hydrogen atom already residing at the surface. Where at least some surface diffusion is possible, dimers can form from adatoms deposited at larger separations. For example, when the mean hydrogen free path during a lifetime is ∼10 interatomic distances, the formation of dimers from predeposited hydrogen monomers requires the coverage of ∼1%. The formation of big hydrogen nanoislands simply by agglomeration of predeposited hydrogen monomers at a coverage in the range of several percent seems improbable. This does not rule out, however, the possibility of controlled growth of nanoislands on graphene or graphite. In fact, hydrogen dimers, because of their higher thermal stability compared with monomers, can be used as the cluster nuclei. Experiments on dimer formation[23,34,36] clearly demonstrate the possibility of tuning the density of dimers by a proper adjustment of the deposition dose and annealing regime. Subsequently, bigger clusters could be grown from these nuclei by hydrogen deposition with a careful balance of substrate temperature and deposition rate. Ideally, monomers deposited close to the clusters should be able to reach the latter by surface diffusion, whereas those deposited far from clusters would be released more quickly than new atoms in their vicinity appear, so that the nucleation of additional clusters would be avoided.

Because of the importance of the hydrogen-carbon interaction for astrophysical problems, wherein relevant temperatures are well below room temperature, a considerable part of the available experimental data relates to low temperatures. It makes sense to discuss briefly in which respects the hydrogen interaction with "hot" carbon samples (as studied in particular in this paper) differs from that with "cold" samples.

A known problem of hydrogen deposition onto a perfectly flat graphite/graphene surface is the necessity for a hydrogen atom to overcome an adsorption energy barrier. To stick to a "cold" graphene sheet, the hydrogen atom itself must be "hot" (i.e., have kinetic energy at least comparable to the barrier height of ∼0.2 eV); otherwise, hydrogen absorption is completely suppressed (e.g., Ref. 66 and references therein). On the contrary, in our simulations, a detached hydrogen atom seems to have no problem attaching back onto the graphene sheet. As can be seen in Fig. 6, at 2000 K, approximately half of the free hydrogen atom collisions with graphene results in hydrogen

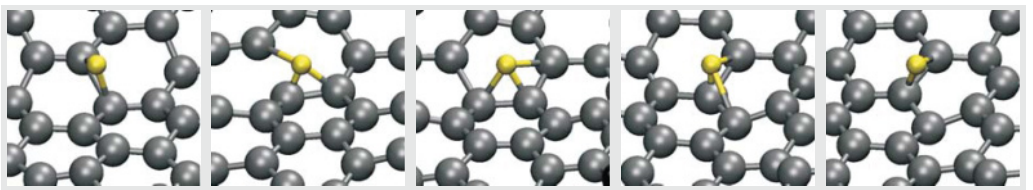

FIG. 16. (Color online) Several consecutive hydrogen atom configurations within the same diffusion jump in MD-DFT simulations.

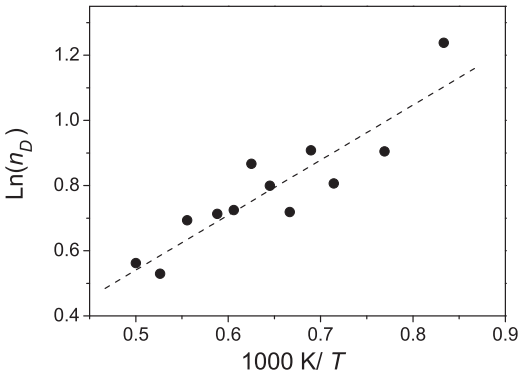

FIG. 17. Dependence of the average number of hydrogen jumps per lifetime, n_D, on the inverse temperature, as predicted by MD simulations with the Brenner potential. The dashed line (with slope corresponding to an activation energy of 0.15 eV) is the least squares fit.

capture. Even at the lowest considered temperature, hydrogen atoms are easily recaptured. Keeping in mind that at high temperatures graphene is strongly corrugated, it is not even clear whether any hydrogen adsorption barrier exists at all.

Another difference is the angular distribution of detached hydrogen atoms. As discussed in Sec. III A, a hydrogen atom does not necessarily move strictly normal to the graphene surface to detach from its carbon neighbor. However, the difference between detachment barriers for a hydrogen atom moving normally to the surface and, say, along a carbon hexagon diagonal is on the order of 0.3 eV. That is, it can be expected that detrapping trajectories normal to the graphene surface dominate at and below the room temperature. On the contrary, at temperatures above 1200 K, the observed hydrogen fly-off directions are essentially random.

Commonly, little difference is expected between hydrogen interaction with a graphene monolayer and a monocrystalline graphite surface. Many aspects of the hydrogen interaction with carbon surfaces have been experimentally studied on highly oriented pyrolytic graphite (HOPG). Graphite can be easily heated up (in a vacuum) to the temperatures considered in this work, so the study of hydrogen-graphite interaction is not restricted to low temperatures. In some experiments (e.g., those on chemisorbed hydrogen desorption in molecular[67] or atomic[68] form), the local heating of HOPG surfaces by pulsed laser irradiation reached 1900 K, so it makes sense to discuss to which extent the results obtained on graphite samples are relevant for hydrogen interaction with freely suspended graphene, as studied here.

The representation of the top layer of a (0001) surface of monocrystalline graphite with a graphene monolayer seems very reasonable at room temperature and below, but at temperatures of many hundreds of degrees Kelvin, the transferability of results between graphene and graphite is not obvious. As can be seen in Fig. 13(a), already at 1200 K, carbon atom vibration amplitudes perpendicular to the graphene plane reach ∼1.5 Å, which is nearly half the distance between graphite planes. Evidently, at such high temperatures, the interaction between graphite planes cannot be neglected. The interplane interaction is expected to affect, among other things, the vibration spectrum of the surface graphite layer, which can be reflected in hydrogen kinetics.

A rough estimate of the limiting temperature, up to which the surface layer of graphite is reasonably approximated as an isolated graphene, can be deduced from a comparison of the thermal expansion behavior of graphene and graphite. At low temperatures, both graphite[49,69,70] and graphene[49,71] are known to contract in-plane with an increase in temperature. However, at temperatures above ∼700 K, in-plane contraction in graphite is replaced by expansion,[49,69,70] whereas graphene is expected to continue contracting to temperatures well above 2000 K.[49] The contraction is promoted by the relative ease of carbon atom displacements normal to the graphene plane,[49] which are able to consume the temperature-induced increase of average distance between carbon atoms. Because the contraction trend persists to very high temperatures in freely suspended graphene, it is natural to assume that the trend reversal in graphite is caused by interplane interaction, which limits the out-of-plane shifts of carbon atoms. Correspondingly, above ∼700 K, one should be cautious when comparing hydrogen dynamics on graphite and graphene.

V. CONCLUSIONS

(1) To verify compatibility of the two MD approaches, we have compared their predictions of "static" hydrogen properties at 0 K. The "classical" potential correctly reproduces the on-top hydrogen location at the graphene sheet as the most stable hydrogen configuration. The "static" binding energies of hydrogen atom to the graphene surface are 1.36 and 0.8 eV for classical potential and DFT calculations, respectively.

(2) Our DFT CI-NEB results for relatively large (160-atom) supercell agree with the earlier calculations in predicting a non-monotonous hydrogen potential energy variation with the increase of hydrogen-graphene separation and detrapping barrier of 1.1 eV at 0 K. On the other hand, hydrogen-carbon bond breaking is shown to be notably more difficult when the carbon layer is allowed to follow the detrapping hydrogen atom. This implies that, in dynamic simulations, the efficient detrapping energy can differ from the "static" value. The dynamic hydrogen detrapping barrier (1.2 eV), defined as the average kinetic energy loss in a detachment event, was indeed found to exceed the "static" barrier, but only slightly. The dynamic hydrogen detrapping barrier of MD-DFT nicely correlates with the activation energy for hydrogen detrapping of 1.26 eV, predicted by simulations with the Brenner semiempirical potential.

(3) The CI-NEB (DFT) predicts that the migration barrier for 1NN hydrogen diffusion jumps on a graphene surface is 1.0 eV, which is 0.1–0.2 eV less than the desorption barrier. In the MD simulations with Brenner potential, a similar energy difference of 0.12 eV is predicted in the temperature range of 1200–2000 K. In other words, both approaches agree that hydrogen diffusion along a graphene surface is strongly limited by detrapping. A hydrogen atom trapped at the surface is able to make, at best, only several jumps before it leaves the surface. This conclusion excludes the long-range diffusion of hydrogen on graphene, as well as those kinetic processes that might rely on it, such as the diffusion-limited precipitation of hydrogen islands. However, already existing hydrogen clusters can capture hydrogen atoms deposited at the distance of several angstroms from the cluster border.

Hence, short-range surface migration can contribute to the experimentally observed formation of hydrogen pairs from monomer adatoms when hydrogen coverage reaches the level of several percent.

(4) Both approaches predict the existence of rather sophisticated modes for hydrogen transport on graphene. In addition to simple jumps between 1NN carbon atoms, chains of correlated diffusion jumps over two, three, and more C-C bonds constitute a non-negligible part of all diffusion events. In DFT-MD, one observes also particularly long-distance "ballistic" jumps of hydrogen atoms, resulting from unsuccessful detrapping attempts. The latter jumps are, however, too rare to noticeably contribute to hydrogen transport along the graphene surface.

(5) A by-product of the current simulations is the discovery of a self-organized sinusoidal vibration instability of graphene at high temperatures (at least up to 1500 K). The effect was not studied here in depth, being not directly related to the main topic of the paper (except that hydrogen transport is completely suppressed in the well-developed sinusoidal vibration mode). It has been verified, however, that the effect is reproducible and is noticeably promoted by graphene stretching. Providing self-supported graphene oscillations in the terahertz range, the effect could be of interest for practical applications.

ACKNOWLEDGMENTS

We are grateful to Kai Nordlund (University of Helsinki, Finland) for providing us with PARCAS MD code and Laura Oikkonen for carefully checking the manuscript. The research has been supported in part by the Academy of Finland through the Centers of Excellence program (2006–2011) and in part by Grant No. 10-08-90041 from the Russian Foundation for Basic Research. We also thank the Center for Scientific Computing (Helsinki, Finland) and the GRID computational center of NRC "Kurchatov Institute" for the use of their computational facilities.

*borodin@dni.polyn.kiae.su

[1] A. K. Geim and K. S. Novoselov, Nat. Mater. **6**, 183 (2007).
[2] A. K. Geim, Science **324**, 1530 (2009).
[3] M. H. F. Sluiter and Y. Kawazoe, Phys. Rev. B **68**, 085410 (2003).
[4] J. O. Sofo, A. S. Chaudhari, and G. D. Barber, Phys. Rev. B **75**, 153401 (2007).
[5] D. C. Elias, R. R. Nair, T. M. G. Mohiuddin, S. V. Morozov, P. Blake, M. P. Halsall, A. C. Ferrari, D. W. Boukhvalov, M. I. Katsnelson, A. K. Geim, and K. S. Novoselov, Science **323**, 610 (2009).
[6] D. R. Dreyer, R. S. Ruoff, and C. W. Bielawski, Angew. Chem. Int. Ed. Engl. **49**, 9336 (2010).
[7] L. Liu and Z. Shen, Appl. Phys. Lett. **95**, 252104 (2009).
[8] S. Lebègue, M. Klintenberg, O. Eriksson, and M. I. Katsnelson, Phys. Rev. B **79**, 245117 (2009).
[9] M. Topsakal, S. Cahangirov, and S. Ciraci, Appl. Phys. Lett. **96**, 091912 (2010).
[10] R. Balog, B. Jørgensen, L. Nilsson, M. Andersen, E. Rienks, M. Bianchi, M. Fanetti, E. Lægsgaard, A. Baraldi, S. Lizzit, Z. Sljivancanin, F. Besenbacher, B. Hammer, T. G. Pedersen, P. Hofmann, and L. Hornekær, Nat. Mater. **9**, 315 (2010).
[11] D. Haberer, D. V. Vyalikh, S. Taioli, B. Dora, M. Farjam, J. Fink, D. Marchenko, T. Pichler, K. Ziegler, S. Simonucci, M. S. Dresselhaus, M. Knupfer, B. Büchner, and A. Grüneis, Nano Lett. **10**, 3360 (2010).
[12] E. J. Duplock, M. Scheffler, and P. J. D. Lindan, Phys. Rev. Lett. **92**, 225502 (2004).
[13] O. V. Yazyev and L. Helm, Phys. Rev. B **75**, 125408 (2007).
[14] S. Casolo, O. M. Løvvik, R. Martinazzo, and G. F. Tantardini, J. Chem. Phys. **130**, 054704 (2009).
[15] P. Sessi, J. R. Guest, M. Bode, and N. P. Guisinger, Nano Lett. **9**, 4343 (2009).
[16] T. O. Wehling, M. I. Katsnelson, and A. I. Lichtenstein, Phys. Rev. B **80**, 085428 (2009).
[17] G. Buchs, A. V. Krasheninnikov, P. Ruffieux, P. Gröning, A. S. Foster, R. M. Nieminen, and O. Gröning, New J. Phys. **9**, 275 (2007).
[18] T. T. Vehviläinen, M. G. Ganchenkova, V. A. Borodin, and R. M. Nieminen, J. Nanosci. Nanotechn. **9**, 4246 (2009).
[19] P. Chandrachud, B. S. Pujari, S. Haldar, B. Sanyal, and D. G. Kanhere, J. Phys. Condens. Matter **22**, 465502 (2010).
[20] D. W. Boukhvalov and M. I. Katsnelson, J. Phys. Chem. C **113**, 14176 (2009).
[21] V. V. Ivanovskaya, A. Zobelli, D. Teillet-Billy, N. Rougeau, V. Sidis, and P. R. Briddon, Eur. Phys. J. B **76**, 481 (2010).
[22] H. McKay, D. J. Wales, S. J. Jenkins, J. A. Verges, and P. L. de Andres, Phys. Rev. B **81**, 075425 (2010).
[23] L. Hornekær, E. Rauls, W. Xu, Ž. Šljivančanin, R. Otero, I. Stensgaard, E. Lægsgaard, B. Hammer, and F. Besenbacher, Phys. Rev. Lett. **97**, 186102 (2006).
[24] D. W. Boukhvalov, M. I. Katsnelson, and A. I. Lichtenstein, Phys. Rev. B **77**, 035427 (2008).
[25] R. Ströbel, J. Garche, P. T. Moseley, L. Jörissen, and G. Wolf, J. Power Sources **159**, 781 (2006).
[26] Y. Lin, F. Ding, and B. I. Yakobson, Phys. Rev. B **78**, 041402(R) (2008).
[27] A. Ranjbar, M. S. Bahramy, M. Khazaei, H. Mizuseki, and Y. Kawazoe, Phys. Rev. B **82**, 165446 (2010).
[28] T. Zecho, A. Güttler, X. Sha, B. Jackson, and J. Küppers, J. Chem. Phys. **117**, 8486 (2002).
[29] T. Zecho, A. Güttler, and J. Küppers, Carbon **42**, 609 (2004).
[30] P. Ruffieux, O. Gröning, P. Schwaller, L. Schlapbach, and P. Gröning, Phys. Rev. Lett. **84**, 4910 (2000).
[31] P. Ruffieux, O. Gröning, M. Bielmann, P. Mauron, L. Schlapbach, and P. Gröning, Phys. Rev. B **66**, 245416 (2002).
[32] L. Jeloaica and V. Sidis, Chem. Phys. Lett. **300**, 157 (1999).
[33] E. Aréou, G. Cartry, J.-M. Layet, and T. Angot, J. Chem. Phys. **134**, 014701 (2011).
[34] L. Hornekær, Ž. Šljivančanin, W. Xu, R. Otero, E. Rauls, I. Stensgaard, E. Lægsgaard, B. Hammer, and F. Besenbacher, Phys. Rev. Lett. **96**, 156104 (2006).
[35] Z. M. Ao and F. M. Peeters, Appl. Phys. Lett. **96**, 253106 (2010).
[36] A. Andree, M. Le Lay, T. Zecho, and J. Küpper, Chem. Phys. Lett. **425**, 99 (2006).

[37]R. Balog, B. Jørgensen, J. Wells, E. Lægsgaard, P. Hofmann, F. Besenbacher, and L. Hornekær, J. Am. Chem. Soc. **131**, 8744 (2009).
[38]X. Sha and B. Jackson, Surf. Sci. **496**, 318 (2002).
[39]Y. Ferro, F. Marinelli, and A. Allouche, Chem. Phys. Lett. **368**, 609 (2003).
[40]L. F. Huang, M. Y. Ni, X. H. Zheng, W. H. Zhou, Y. G. Li, and Z. Zeng, J. Phys. Chem. C **114**, 22636 (2010).
[41]Y. Ferro, F. Martinelli, A. Jelea, and A. Allouche, J. Chem. Phys. **120**, 11882 (2004).
[42]L. Chen, A. C. Cooper, G. P. Pez, and H. Cheng, J. Phys. Chem. C **111**, 18995 (2007).
[43]C. P. Herrero and R. Ramírez, Phys. Rev. B **79**, 115429 (2009).
[44]D. W. Boukhvalov, Phys. Chem. Chem. Phys. **12**, 15367 (2010).
[45]Y. Lei, S. A. Shevlin, W. Zhu, and Zh. X. Guo, Phys. Rev. B **77**, 134114 (2008).
[46]K. Nordlund, PARCAS computer code (2006).
[47]D. W. Brenner, Phys. Rev. B **42**, 9458 (1990).
[48]H. J. C. Berendsen, J. P. M. Postma, W. F. van Gunsteren, A. DiNola, and J. J. R. Haak, J. Chem. Phys. **81**, 3684 (1984).
[49]N. Mounet and N. Marzari, Phys. Rev. B **71**, 205214 (2005).
[50]A. Fasolino, J. H. Los, and M. I. Katsnelson, Nature Mater. **6**, 858 (2007).
[51]J. H. Los, M. I. Katsnelson, O. V. Yazyev, K. V. Zakharchenko, and A. Fasolino, Phys. Rev. B **80**, 121405(R) (2009).
[52]F. L. Braghin and N. Hasselmann, Phys. Rev. B **82**, 035407 (2010).
[53]J. C. Meyer, A. K. Geim, M. I. Katsnelson, K. S. Novoselov, T. J. Booth, and S. Roth, Nature **446**, 60 (2007).
[54]G. Kresse and J. Hafner, Phys. Rev. B **47**, 558 (1993).
[55]G. Kresse and J. Furthmüller, Phys. Rev. B **54**, 11169 (1996).
[56]J. P. Perdew, K. Burke, and M. Ernzerhof, Phys. Rev. Lett. **77**, 3865 (1996).
[57]P. E. Blöchl, Phys. Rev. B **50**, 17953 (1994).
[58]G. Kresse and D. Joubert, Phys. Rev. B **59**, 1758 (1999).
[59]H. J. Monkhorst and J. D. Pack, Phys. Rev. B **13**, 5188 (1976).
[60]G. Henkelman, B. P. Uberuaga, and H. Jonssón, J. Chem. Phys. **113**, 9901 (2000).
[61]R. Johnson and J. Beeler, in *Interatomic Potentials and Crystalline Defects*, edited by J. K. Lee (The Metallurgical Society of AIME, Warrendale, PA, 1981), p. 165.
[62]P. O. Lehtinen, A. S. Foster, Y. Ma, A. V. Krasheninnikov, and R. M. Nieminen, Phys. Rev. Lett. **93**, 187202 (2004).
[63]F. Liu, P. Ming, and J. Li, Phys. Rev. B **76**, 064120 (2007).
[64]B. Rakshit and P. Mahadevan, Phys. Rev. B **82**, 153407 (2010).
[65]C. A. Marianetti and H. G. Yevick, Phys. Rev. Lett. **105**, 245502 (2010).
[66]S. Morisset, Y. Ferro, and A. Allouche, J. Chem. Phys, **133**, 044508 (2010).
[67]S. Baouche, G. Gamborg, V. V. Petrunin, A. C. Luntz, A. Baurichter, and L. Hornekær, J. Chem. Phys. **125**, 084712 (2006).
[68]S. Baouche, L. Hornekær, A. Baurichter, A. C. Luntz, V. V. Petrunin, and Ž. Šljivančanin, J. Chem. Phys. **131**, 244707 (2009).
[69]J. B. Nelson and D. P. Riley, Proc. Phys. Soc. London **57**, 477 (1945).
[70]D. P. Riley, Proc. Phys. Soc. London **57**, 486 (1945).
[71]W. Bao, F. Miao, Z. Chen, H. Zhang, W. Jang, C. Dames, and C. N. Lau, Nature Nanotech. **4**, 562 (2009).